Mem. Natl Inst. Polar Res., Spec. Issue, 48, 134–160, 1987

HEMISPHERIC ASYMMETRIES IN THERMOSPHERIC STRUCTURE AND DYNAMICS

David REES and Timothy J. FULLER-ROWELL

Department of Physics and Astronomy, University College London, Gower Street, London WC1E 6BT, U.K.

Abstract: Hemispheric differences in the structure and dynamics of the polar regions of the thermosphere and ionosphere are caused by seasonal/latitudinal asymmetries of solar insolation acting in addition to the effects of the distinctive asymmetries of the main geomagnetic field. Viewing the earth from a satellite, the longitudinal and universal time variations of the thermosphere and ionosphere are far more spectacular in the southern polar thermosphere and ionosphere than in the northern polar regions. This is simply caused by the greater offset of the geomagnetic pole from the geographic pole in the southern hemisphere, and the associated geomagnetic forcing of the polar thermosphere and ionosphere. The southern polar cusp is a localised region of intense forcing with a diurnal migration in geographic latitude from 55° to the southern geographic pole. At times of major geomagnetic disturbances, the combination of the equatorward expansion of the auroral oval and the greater offset of the southern geomagnetic pole from the rotational pole causes dramatic effects in southern mid-latitude and near-equatorial regions. The northern auroral oval rarely expands within 40° of the equator (at mid-American longitudes). In the Australian sector, equivalent major geomagnetic disturbances may extend to a southern latitude of 30°. Wind, gravity wave and ionospheric perturbations originating in the auroral ovals decrease rapidly in amplitude with increasing distance from the source region. The greater frequency and amplitude of auroral-related disturbances reaching a particular mid- or low-latitude region in the southern hemisphere, particularly in the Australian sector is thus explained. A survey of recent satellite data will be presented, highlighted by simulations using a global theoretical model, to demonstrate the causes of these hemispheric asymmetries. Future complementary ground-based and space measurements can exploit the hemispheric asymmetries to clearly identify geomagnetic forcing mechanisms. The greater UT and latitudinal modulation in the southern hemisphere may be used to identify sub-auroral excitation of the thermosphere and ionosphere during major storms. The cause of the related negative *F*-region storm-time response is still not certain, even after 30 years of study.

1. Introduction

The annual modulation of solar insolation, due to the eccentricity of the earth's orbit around the sun, and the associated variation of solar photoionising radiation, on a global scale, is relatively small. With this exception, the major external energy inputs which generate the fundamental structure and behaviour of the low and middle-latitude thermosphere and ionosphere are quite symmetric about the equator at the

equinox. Seasonal/latitudinal, and hemispheric variations of solar forcing are also symmetric with respect to geographic latitude.

This seasonal and hemispheric symmetry is observed in the most general properties of the thermosphere, *i.e.* density and temperature, during quiet geomagnetic conditions, at low latitudes. Progressing to higher latitudes, and during periods influenced by significant geomagnetic disturbances, the thermosphere shows large UT and hemispheric asymmetries, which are clearly largest in the geomagnetic polar regions.

The ionosphere, however, is strongly influenced, even at very low and equatorial latitudes, by the main geomagnetic field. Despite the relative symmetry of the low-latitude thermosphere to solar forcing, the influence of the geomagnetic field ensures that the major low-latitude ionospheric diurnal and seasonal responses can only be understood by considering the combined influences of thermospheric winds and ionospheric electric fields. The ionospheric effects (plasma transport) of both are strongly related to the strength and direction of the local geomagnetic field. Many hemispheric/longitudinal asymmetries of the ionosphere are determined by the quite different geomagnetic field orientations at most locations of comparable geographic latitude and longitude in the northern and southern hemispheres, that is, where the local heating and ionising inputs from solar UV and EUV are otherwise quite symmetric.

Progressing to higher geographic latitudes, the combined influence of symmetric solar forcing and asymmetric geomagnetic field control or modulation can still be observed. However, in both hemispheres, the geomagnetic latitude (defined alternatively by dip-latitude, or by "L" shell) becomes an increasingly important feature. At geomagnetic latitudes of around 60° or higher, the behaviour of the ionosphere is no longer solar-dominated (*i.e.* related to the intensity of solar ionising radiation). Poleward of a geomagnetic latitude of about 65°, the structure and dynamics of the thermosphere and the ionosphere response are dominated by processes which do not correspond closely to seasonal and latitudinal variations of solar insolation. These departures are quite noticeable during relatively quiet geomagnetic periods. During disturbed geomagnetic periods, the response of the high-latitude ionosphere and thermosphere can, at first sight, appear to be chaotic. Isolated observations from single locations are difficult to interpret. However, combined observations from many stations, obtained over a wide range of seasonal, solar and geomagnetic activity, the data from spacecraft, and from many recent coordinated large-scale observing programmes, coupled with advances in theoretical and numerical modelling, have provided a viable framework for understanding the majority of major phenomena observed in both the ionosphere and thermosphere.

The strong response of the polar thermosphere and ionosphere to geomagnetic forcing was recognised early in the history of space exploration of the upper atmosphere (JACCHIA, 1959, 1961) and the global response to geomagnetic activity was documented in the semi-empirical models (*i.e.* JACCHIA, 1977). The causes of the geomagnetic variation were understood to be a combination of Joule heating (COLE, 1962, 1971) and auroral energetic particle heating at high latitudes. The existence of strong electric fields at high geomagnetic latitudes, capable of generating the large storm-time ionospheric currents, had been earlier predicted (AXFORD and HINES, 1961; DUNGEY,

1961) as a result of the interaction between the solar wind and the magnetosphere and had been observed by high latitude rocket experiments. The OGO-6 spacecraft provided the first global observations of the polar electric field distribution (Heppner, 1972, 1977). These observations showed that the polar convection electric field was persistent, and not an exclusive feature of geomagnetic disturbances. Energetic particle precipitation, already well known as the cause of the visible aurora before the start of the Space Era, was observed by the first satellites. Global maps of the distribution from satellites was not, however, available until the empirical models of Spiro *et al.* (1982), Hardy *et al.* (1985) were produced.

Experimental observations which illustrate clearly the thermospheric response to geomagnetic processes and activity have been obtained from Dynamics Explorer-2 (Hays *et al.*, 1984; Killeen *et al.*, 1982, 1984; Rees *et al.*, 1983a, b, 1985a, 1986) and from ground-based Fabry-Perot interferometers (GBFPI) (Rees *et al.*, 1980, 1982, 1984a, 1985b). The DE-2 data document the polar and general high latitude response to a range of geomagnetic disturbances, particularly that of the southern geographic and geomagnetic polar regions. GBFPI observations, from high latitude stations in the northern hemisphere, recorded the frequent perturbation of the polar regions by moderate to large geomagnetic disturbances, while mid-latitude stations were able to observe the effects of rarer major geomagnetic events. Some GBFPI data has recently been available from the southern hemisphere polar regions (Stewart *et al.*, 1985). These data show that the fundamental framework of interpreting the dynamical behaviour of the thermosphere in the southern hemisphere is similar to that of the northern hemisphere. However, the data from Halley Bay also indicate some dynamical responses which may be characteristic of the large offset between geographic and geomagnetic poles in the southern hemisphere, and which are thus unique to the southern hemisphere.

Theoretical three dimensional and time-dependent global models of the earth's thermosphere have been developed by Fuller-Rowell and Rees (1980, 1983), by Dickinson *et al.* (1981) and Roble *et al.* (1982, 1983). Global simulations of the structure and dynamics of the thermosphere require realistic values of the energetic input from the UV and EUV components of solar radiation (Hinteregger, 1981) and of the UV and EUV heating efficiency (Torr *et al.*, 1980).

A realistic global description of the thermosphere also requires the inclusion of the highly variable energy and momentum inputs from the solar wind via the earth's magnetosphere since, during disturbed periods, the local heating rates and momentum transfer rates from magnetospheric sources can be more than two orders of magnitude greater than those due to the low latitude solar UV and EUV heating, and an order of magnitude greater in quiet periods. The structure and dynamics of the polar thermosphere is thus strongly modified by the signatures of magnetospheric processes, even during relatively quiet geomagnetic periods. The thermospheric response resulting from intense energy and momentum sources associated with geomagnetic forcing can be simulated by the inclusion of a polar convection electric field, and by the self-consistent enhancement of the polar ionosphere and the polar energy input resulting from magnetospheric precipitation. The validity of appropriate model simulations has been tested by comparison with data sets from spacecraft such as Dynamics Explorer

(REES *et al.*, 1983a, 1985a, b, 1986), from incoherent scatter radars (REES *et al.*, 1984a), and from ground-based Fabry-Perot interferometers located at high latitude stations (REES *et al.*, 1983b, 1984b).

Major features of the seasonal/latitudinal response of the thermosphere which appear in these simulations, and which are of fundamental importance to the ionosphere include the effects of large compositional changes at a fixed pressure level, in addition to the effects of large and variable thermospheric winds. The compositional changes respond to geomagnetic forcing, which amplifies the seasonal effect. The thermospheric compositional changes dramatically modify the feed-back between the thermosphere and ionosphere, particularly during periods of high geomagnetic activity. As a result, it has become necessary to develop self-consistent coupled models of the ionosphere and thermosphere, in order to obtain a detailed understanding of the relative importance of competitive forcing mechanisms and the feed-back processes. A brief review of progress in these areas will be given. More comprehensive treatments can be found in FULLER-ROWELL *et al.* (1987a, b), FULLER-ROWELL (1987), and REES and FULLER-ROWELL (1987a, b).

2. Theoretical Modelling of the Thermosphere and Ionosphere

The UCL-3D thermospheric model simulates the time-dependent structure of the vector wind, temperature, density and composition of the neutral atmosphere, by numerically solving the non-linear equations of momentum, energy and continuity (FULLER-ROWELL and REES, 1980), and a time-dependent mean mass equation (FULLER-ROWELL and REES, 1983). The global atmosphere is divided into a series of elements in geographic latitude, longitude and pressure. Each grid point rotates with the earth to define a non inertial frame of reference in a spherical polar coordinate system. The latitude resolution is 2°, the longitude 18°, and each longitude slice sweeps through all local times with a 1 min time step. In the vertical direction the atmosphere is divided into 15 levels in log pressure, each layer equivalent to one scale height thickness, from a lower boundary of 1 Pa at 80 km altitude.

In the thermospheric model, the top pressure level varies in altitude with changes in the temperature profile from around 300 km during extremely quiet geomagnetic periods at low solar activity, to altitudes in excess of 700 km during disturbed periods at high solar activity. In all cases, the range of pressure levels covers the thermospheric regimes from below the mesopause, up to and including altitudes where there are only small vertical gradients of neutral velocity and temperature, in the vicinity of the exobase. Similarly, the pressure or altitude range covers the ionospheric *E*- and *F*-regions. Most of the simulations to be described here rely on empirical descriptions of ion density from CHIU (1975), with high latitude plasma density enhancements to simulate the effects of auroral precipitation during periods of disturbed geomagnetic activity. A recently-developed self-consistent coupled ionosphere-thermosphere model (FULLER-ROWELL *et al.*, 1987a, b) describes realistically the interdependence of ionospheric and thermospheric parameters, of particular importance at high geomagnetic latitudes. The results of two simulations using this coupled model will be briefly discussed.

The time-dependent variables of southward and eastward neutral winds, total

energy density, and mean molecular mass are evaluated at each grid point by an explicit time stepping numerical technique. After each iteration the vertical wind is derived, together with temperature, heights of pressure surfaces, density, and atomic oxygen and molecular nitrogen concentrations. The data can be interpolated to fixed heights for comparison with experimental data, or with empirical models.

The momentum equation is non-linear and the solutions fully describe the horizontal and vertical advection, *i.e.* the transport of momentum. The transformation to a non-inertial frame of a rotating spherical atmosphere is complete with the exception that the radial centrifugal component is absorbed within the gravitational acceleration, g, which is assumed constant at 9.5 m s^{-2}. This transformation results in the curvature and Coriolis effects which are fundamental in realistic simulations of atmospheric dynamics. The momentum equation also includes horizontal pressure gradients, described exactly by gradients in the heights of the pressure surfaces, horizontal and vertical viscosity, and ion drag. Similarly, the non-linear energy equation is solved self-consistently with the momentum equation, and it describes the three dimensional advection of energy, and the transfer of energy between internal, kinetic and potential energy. The solutions also describe the horizontal and vertical heat conduction by both molecular and turbulent processes, heating by solar UV and EUV radiation, cooling by infrared radiation, and heating due to the ohmic dissipation of ionospheric currents, known as Joule and frictional heating.

The composition equation, which describes the rate of change of mean molecular mass, is solved self-consistently with the momentum and energy equations, and defines uniquely the concentrations of atomic oxygen and molecular nitrogen. The numerical solution describes the transport of these major species and the relative diffusion by both molecular and turbulent processes throughout the three-dimensional atmosphere. Photo-dissociation of molecular oxygen and chemical processes in the lower thermosphere are not treated explicitly. Evaluation of the respective time-constants, and comparison with experimental data, show that these assumptions are generally realistic. In the upper thermosphere, molecular oxygen density decreases with height slightly faster than molecular nitrogen, and is nearly de-coupled from atomic oxygen, due to the relatively long photo-dissociation and recombination time-constants.

The separation of the geomagnetic poles from the geographic poles causes photo-ionisation in the polar regions to have a large diurnal (UT) variation in both hemispheres at any season, due to the diurnal rotation of each geomagnetic polar region about its respective geographic pole. This causes the ion drag and frictional and Joule heating rates in the polar regions to have a large UT dependency by modulating the load on the magnetospheric dynamo. The UT modulation is larger in the southern hemisphere due to the greater separation between geomagnetic and geographic poles. The seasonal variation of solar photo-ionisation in the polar regions appears to cause a similar seasonal/hemispheric variation of the geomagnetic energy and momentum inputs as, with increasing E region conductivity due to increasing solar illumination, the ionospheric load on the magnetospheric dynamo is increased.

Under steady solar and geomagnetic conditions, a time (UT) dependence in the structure and dynamics of the polar thermosphere is induced by the diurnal rotation of the entire geomagnetic polar regions each UT day about the geographic poles. The

diameter of the auroral oval expands and contracts under the influence of changing conditions in the solar wind, with an associated modulation of the electric potential across the polar cap (which causes higher or lower ion drift velocities, ion drag and frictional or Joule heating). Regions of magnetospheric energetic particle precipitation roughly covary with convection patterns, varying the geographic locations and magnitudes of the signatures of magnetospheric processes dramatically.

Seasonal and latitudinal variations in the vertical profile of turbulence within the mesosphere and lower thermosphere affect the transportation of minor and major constituents, heat, and the selective dissipation of the energy of propagating tides and waves. There is, as yet, little reliable data on its average values, let alone its global and seasonal variability. Tidal and gravity waves propagate from sources within the troposphere, stratosphere and mesosphere into the thermosphere. The upward propagation of these tides and of planetary wave features associated with lower atmospheric meteorology, and the selective dissipation of wave and tidal energy in the upper mesosphere and lower thermosphere, causes significant perturbations within the lower thermosphere, and can be traced at upper thermospheric heights (300 km and above). For the purposes of the simulation discussed here, the propagation of lower atmospheric tides into the thermosphere has not been included, and turbulence is assumed globally uniform, with an altitude profile consistent with the mean vertical transport of heat and minor constituents (*e.g.* atomic oxygen).

Modelling the polar ionosphere and the coupling of ionospheric and thermospheric models are both quite complex tasks (SCHUNK, 1987; SOJKA *et al.*, 1979, 1981; SOJKA and SCHUNK, 1985; QUEGAN *et al.*, 1982; FULLER-ROWELL *et al.*, 1984, 1987a, b). The thermospheric model is computed in a spherical coordinate/pressure level grid system, which rotates with the earth, a numerical framework which is fundamentally at odds with the natural framework within which a model of the polar ionosphere can be generated. For the latter, a "convection-path" framework is necessary, where parcels of ionisation are followed as they are convected ($E \times B$) by the combination of external magnetospheric electric fields, and the co-rotation potential due to the rotation of the earth itself, as seen in a fixed sun-earth reference frame. Parcels of the ionosphere are carried by convection through regions of distinct magnetospheric and solar forcing, and through regions where the fundamental structure and composition of the thermosphere changes, with important consequences for ionospheric evolution. This grid-path framework is not a natural framework for thermospheric modelling. In creating a successful self-consistent coupled model, a sophisticated set of routines is required to ensure that both models always receive the appropriate local update information from the other model.

This may seem a complex and laborious approach. However, even the very first results of simulations using this coupled model have demonstrated the intimate and powerful feed-back processes occurring between the polar thermosphere and ionosphere. As a result, many features are produced which are simply not present in non-coupled models of either the thermosphere or the ionosphere. It is quite inappropriate to extract results from theoretical models (SOJKA and SCHUNK, 1985) which exclude the closely coupled physics of these powerful interactions, or from empirical models, such as MSIS, which do not contain the appropriate physical forcing functions,

and cannot resolve the spatial details of regions of the geomagnetically-controlled thermospheric/ionospheric interactions.

3. Seasonal and Latitudinal Asymmetries

Figure 1 shows the structure of the upper thermosphere (pressure level 12, about 320 km), at 18 UT, for a high level of solar activity ($F_{10.7}$ cm=185), and at equinox, for a level of moderate geomagnetic activity ($Kp \sim 2$). Note that the level is not the 165 indicated on this figure itself and following figures. The low latitude regions are relatively symmetric about the geographic equator, and it is only within 30° of the geomagnetic poles that the upper thermospheric wind and temperature distributions show strong traces of the influence of geomagnetic processes. This particular simulation is 'steady-state', in that the only time-dependence is due to the diurnal migration of the geomagnetic polar regions around the geographic poles.

As the geomagnetic polar regions are carried around the geographic poles, the level of photo-ionisation within the auroral oval and polar cap is modulated, changing conductivities, ion drag and electrojet (and other) ionospheric currents. The magnetospheric energy deposition rate in either polar region thus shows considerable diurnal modulation, and a further and larger seasonal modulation.

This is emphasised by Figs. 2 and 3, which are taken from simulations for the December and June solstices, for the same levels of solar and geomagnetic activity as used in Fig. 1.

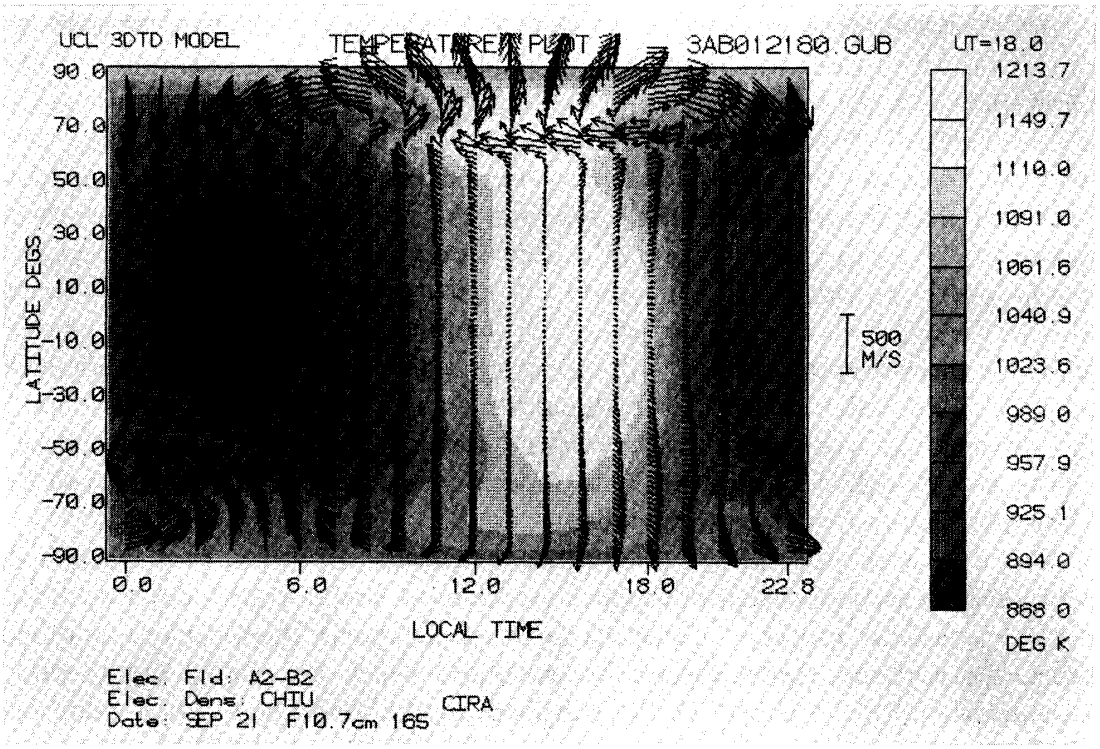

Fig. 1. Upper thermospheric wind and temperature structure (pressure level 12, about 320 km) for a high level of solar activity ($F_{10.7}$ cm=185), at equinox, for a level of moderate geomagnetic activity (Kp~2). Note that the level is not the 165 indicated on the figure itself.

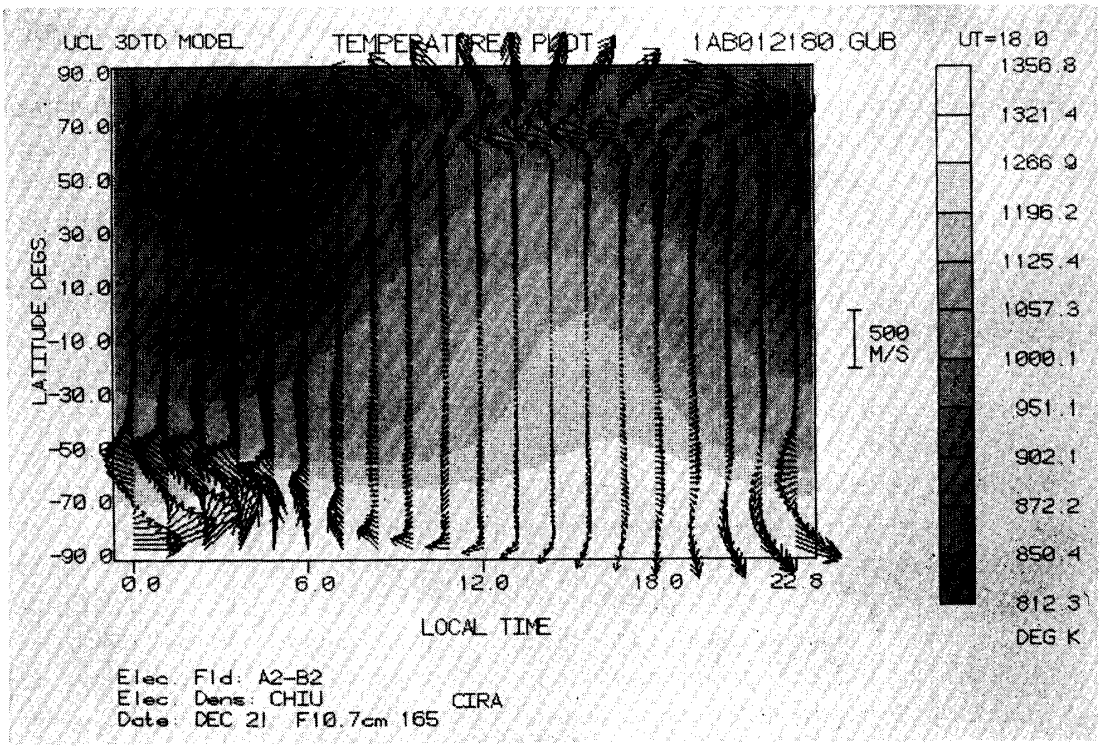

Fig. 2. Same as Fig. 1 but for at the December solstice.

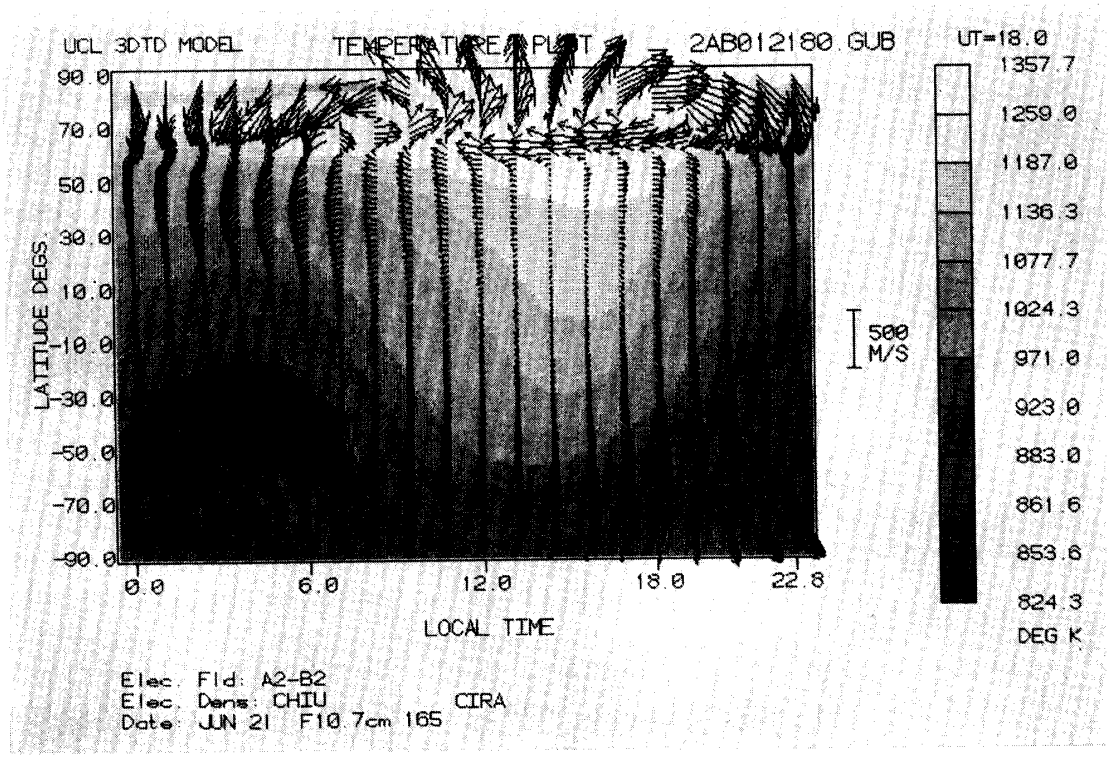

Fig. 3. Same as Fig. 1 but for at the June solstice.

These simulations have been carried out using the global 'CHIU' ionosphere model (1975) to describe the plasma environment, and a polar convection field (70 kV cross-cap potential) from HEPPNER and MAYNARD (1983). No energy from precipitating electrons etc. has been included, and likewise, there is no enhancement of *E*-region conductivities within the auroral oval/polar cap. The models produce a relatively good description of *F*-region winds (REES *et al.*, 1983a, 1985a) for $Kp \sim 2$, but do so by using a polar electric field which is a little too large, and underestimating the overall effects of energetic particle precipitation. The description of *E*-region winds etc. is not as realistic as that of the *F*-region.

These three figures demonstrate the major seasonal/latitudinal (or hemispheric) changes which occur at *F*-region altitudes in the thermosphere. The diurnal variation of wind structures is not particularly different in either hemisphere or season, except for the summer to winter mean flow (close to 50 m/s at solstice). This wind change appears subtle when viewed with this global presentation. The underlying thermal changes, more or less from pole to pole at this simulated low geomagnetic activity level, are important. The mean summer to winter flow causes the large latitudinal variation of mean molecular mass. This gradient, under quiet conditions, corresponds to a ratio of about 7:1 in atomic oxygen to molecular nitrogen in the winter polar region (strictly, the ratio is highest at high winter mid-latitudes) compared with less than 0.5:1 at the summer pole (pressure level 12). The seasonal/latitudinal change has fundamental effects in determining the seasonal behaviour of the ionosphere at middle and high latitudes, and as we will see, underpins the response of the polar ionosphere to geomagnetic activity.

4. Seasonal Variations of the Polar Regions Using the Coupled Model

Figures 4 and 5 show the northern polar cap at winter solstice, at 06 and at 18 UT, respectively, as simulated using the fully-coupled ionospheric-thermospheric model. The simulation has been tuned to a geomagnetic activity level of $Kp=3$, and for a level of high solar activity ($F_{10.7}$ cm = 185), as described in FULLER-ROWELL *et al.* (1987a, b) and FULLER-ROWELL (1987).

The large-scale distribution of mean molecular mass is largely controlled by global circulation, similar to the situation generated by the generic non-self consistent simulations shown in Figs. 1, 2 and 3. The primary result of a self-consistent handling of the high-latitude ionosphere/thermosphere interactions in the presence of moderate geomagnetic activity has been to increase polar heating, primarily as a result of increased *E*-region conductivities. The consequent increased polar updraft and associated outflow has created a plateau of elevated mean molecular mass within the winter polar region, corresponding to an enhanced ratio of molecular nitrogen to atomic oxygen. This contrasts with the global minimum in mean molecular mass at winter mid-latitudes.

Superimposed on this polar plateau are more localized features. A minor maximum in mean molecular mass correlates, apparently anomalously, with the centre of the weak neutral flow in the dawn cell. This feature, with an associated temperature minimum, results from the dynamical consequences of inertia, as described above,

where the neutral flow in the dawn cell tends to be divergent. The other, more substantial, peak in mean molecular mass corresponds to the region of elevated temperature over the polar cap, and also to one of many features in the vertical wind (Fig. 4b). It should be remembered, however, that the vertical wind depicted here is the combination of the component driven by horizontal divergence, and that due to the change in height of the pressure surface. The composition changes seen at a constant pressure surface (Fig. 4b) are affected only by the divergence-driven component. Composition changes seen at constant altitude (*i.e.* by a satellite), will reflect the contribution of both components.

The ion density distribution at pressure level 12, close to the *F*-region peak, is also shown in Fig. 4b. The complete auroral oval is just discernable at 06 UT, when the entire geomagnetic polar region is in darkness. This situation is not typical for *F*-region heights, where the plasma density tends to be controlled more by solar ionisation and transport. Only rarely is the effect of auroral precipitation and ionisation observed as a significant enhancement of the *F*-region ion densities. At this UT, however, the geomagnetic polar region has been in darkness for several hours, so that the effects of solar-produced ionisation and its transport are reduced.

Peak ion densities in the late morning (magnetic local time) are found close to the region of peak auroral ionisation rate (at this pressure level). None of the plasma density features appear to correlate particularly well with features in the mean molecular mass distribution. For example, one would expect to observe the effects of an increase in the loss rate of O^+, in regions of enhanced molecular nitrogen density. However, the mean molecular mass near the winter pole (18–19 amu), although higher than that in winter mid-latitudes (16.5 amu), is still well below values seen at the summer pole (22–24 amu, see later figures). At 06 UT, the sub-auroral trough completely encircles the magnetic polar cap, since even within a narrow band of latitudes on the dayside, the trough region is devoid of either solar or particle ionisation sources.

At 18 UT, on the other hand (Fig. 5a, b), the sub-auroral region on the dayside is in sunlight. Consequently, the dayside sub-auroral trough disappears, for a period of several hours either side of 18 UT. This period when the dayside part of the polar cap is in sunlight has important consequences for the overall plasma densities within the polar cap. For several hours around 18 UT, the entire polar cap is accessible to regions of relatively high (solar-produced) plasma density via convection from the dayside. On the contrary, around 06 UT, the encirclement of the polar cap/auroral oval by the sub-auroral trough is complete. Regions of elevated plasma density, caused by photo-ionisation on the dayside, are no longer able to reach the geomagnetic polar cap, so that plasma densities generally decay, depending on the distribution and intensity of auroral precipitation. It appears that this prediction has an observational counterpart in the data recently reported by DE LA BEAUJARDIERE *et al.* (1985), from the combination of ground-based incoherent scatter radar measurements and those from the Dynamics Explorer satellite. SOJKA and SCHUNK (1985), in their simulation of the southern winter (June) polar cap, observed a comparable effect in the UT variation of the sub-auroral trough (allowing for hemispheric and seasonal differences). However, their polar cap trough (their plate 3, 15 UT) is caused by

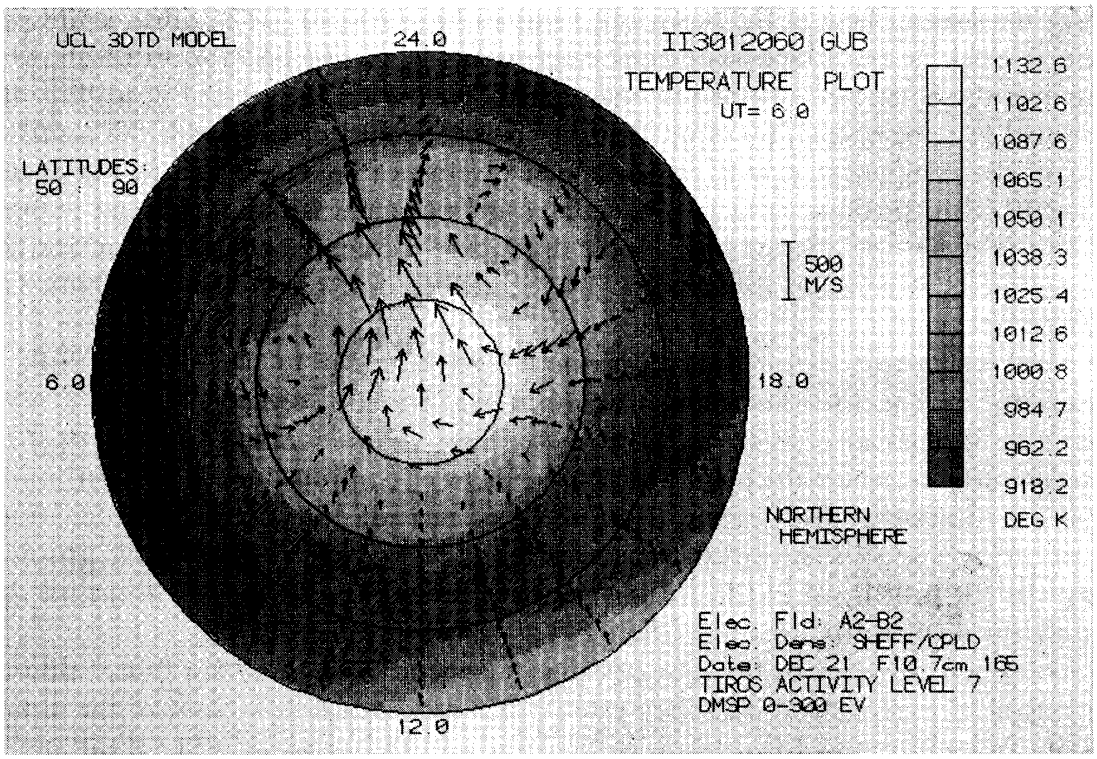

Fig. 4a. Neutral temperature and wind distribution.

Fig. 4. The northern polar cap at winter solstice, at 06 UT, as simulated using the fully-coupled ionospheric-thermospheric model. The simulation has been tuned to a geomagnetic activity level of Kp=3, and for a level of high solar activity ($F_{10.7}$ cm=185). Note that the level is not the 165 indicated on the figure itself.

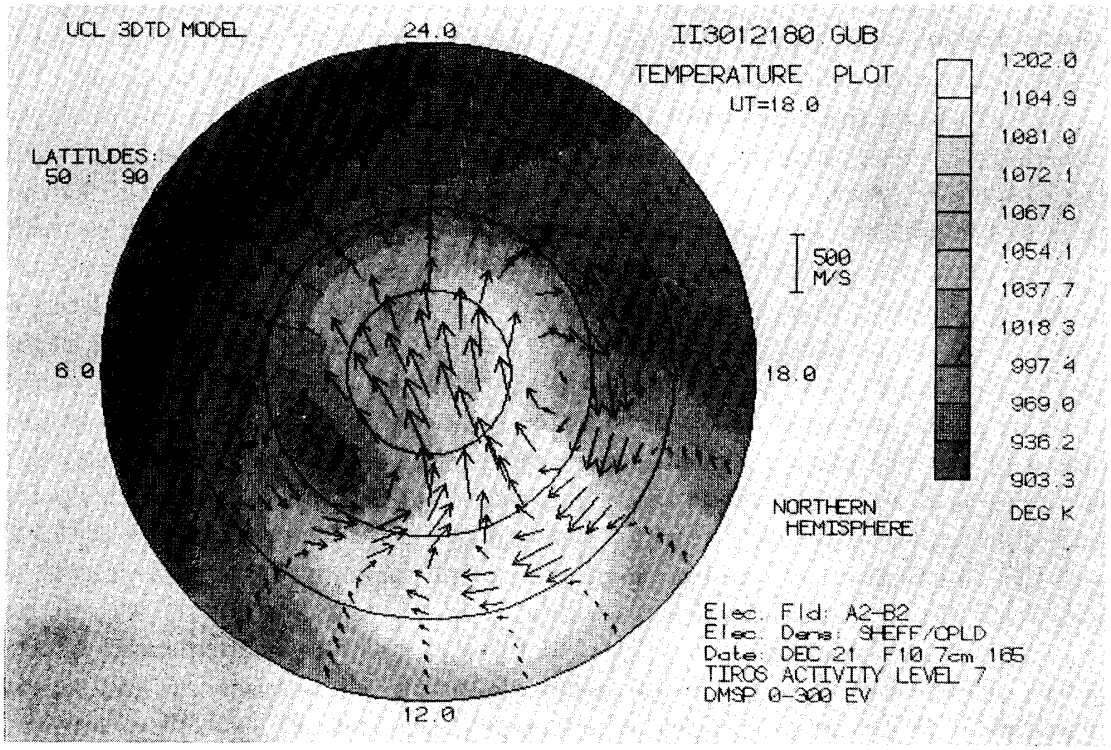

Fig. 5a. Same as Fig. 4a but for at 18 UT.

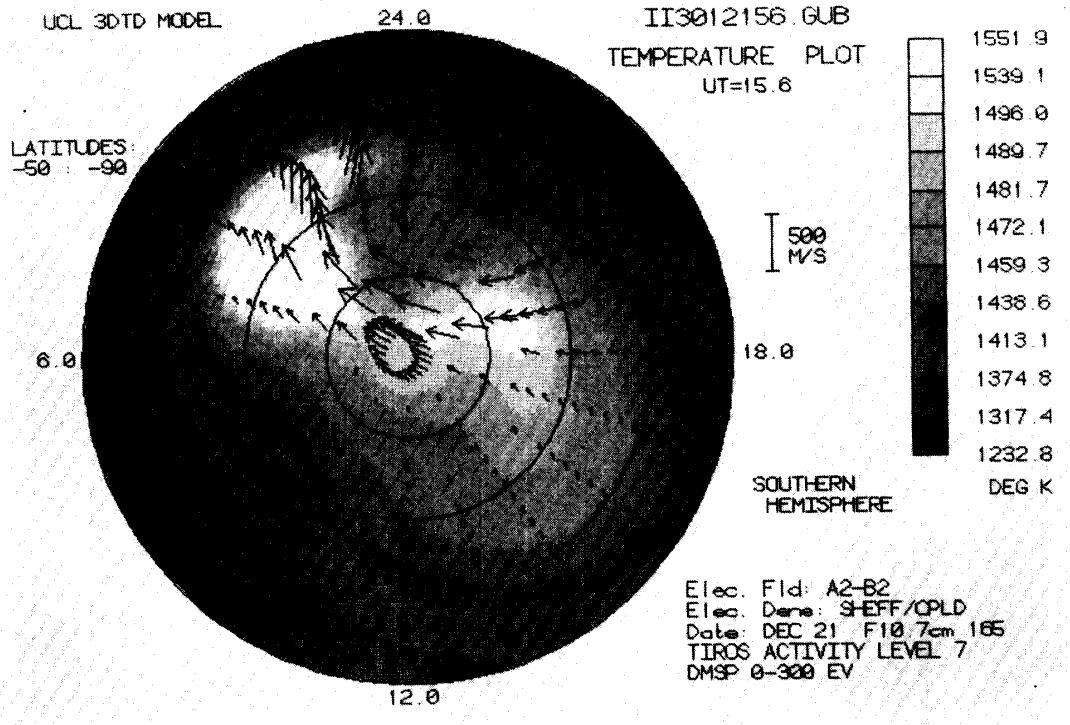

Fig. 6a. Neutral temperature and wind distribution.

Fig. 6. The southern polar cap at the December (southern summer solstice), at 15.6 UT, simulated using the fully-coupled ionospheric-thermospheric model. The simulation has been tuned to a geomagnetic activity level of Kp=3, and for a level of high solar activity ($F_{10.7}$ cm=185). Note that the level is not the 165 indicated on the figure itself.

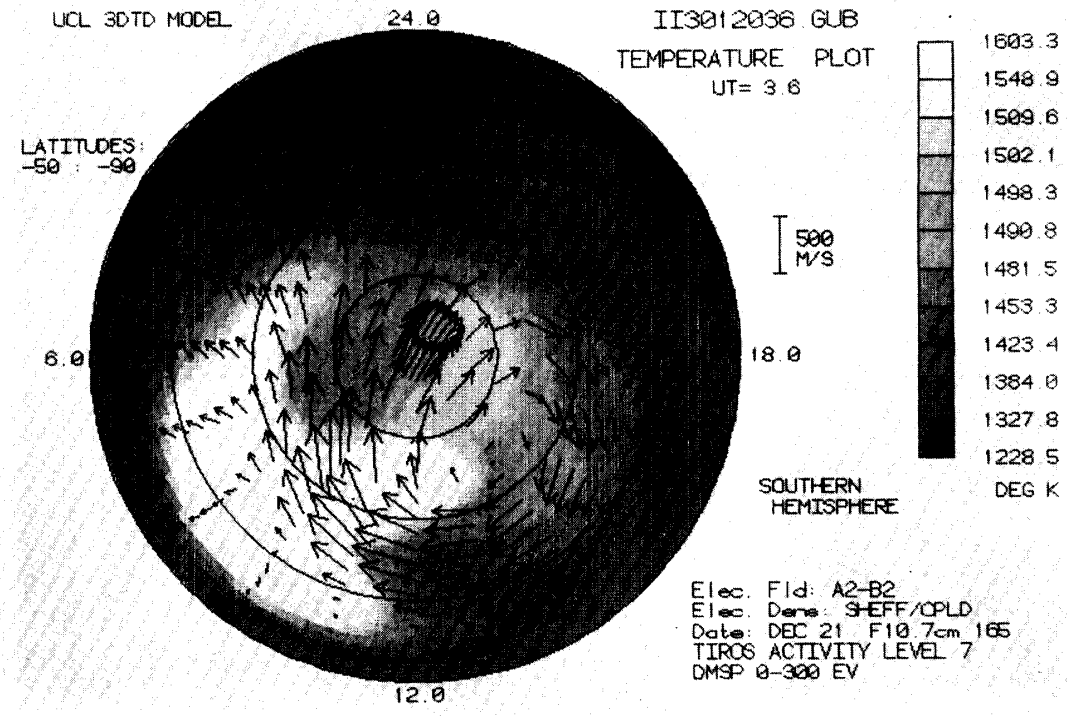

Fig. 7a. Same as Fig. 6a but for at 03.6 UT.

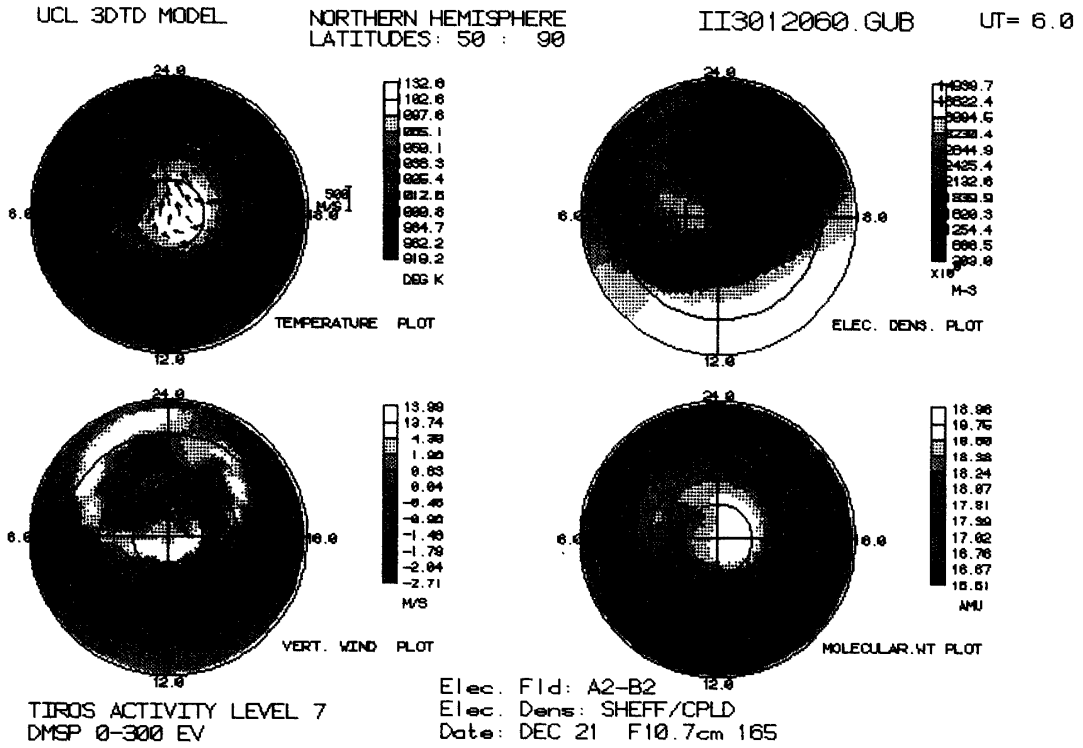

Fig. 4b. The distributions of neutral temperature, vertical wind, mean molecular mass and the ion/electron density.

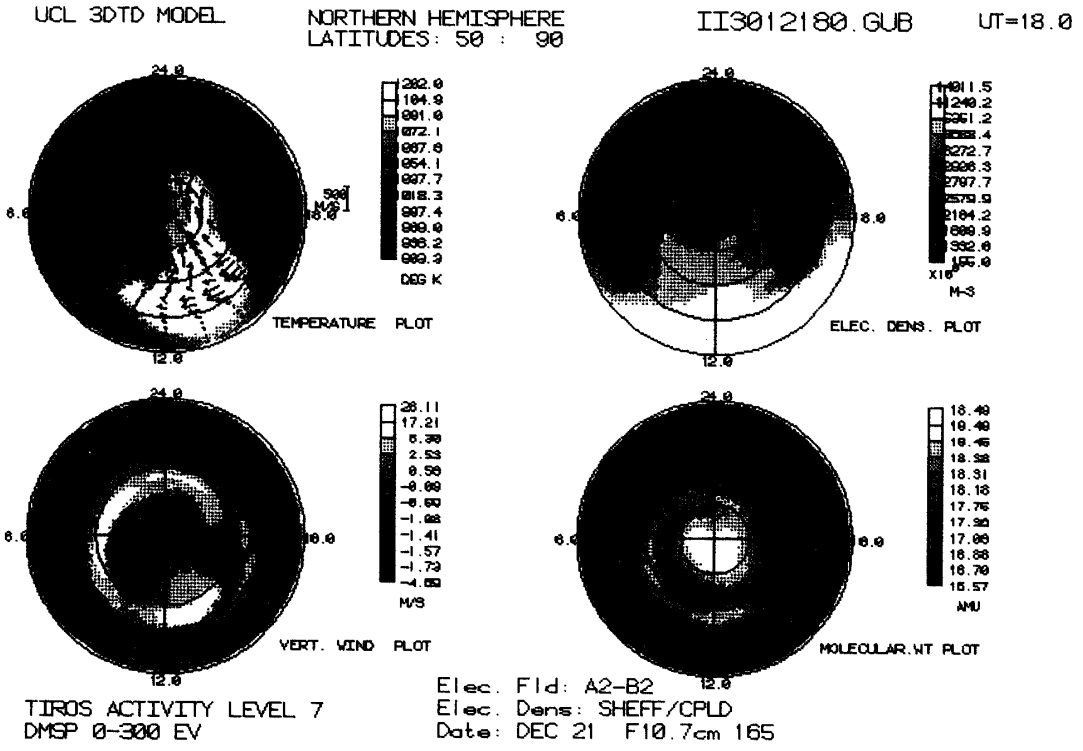

Fig. 5b. Same as Fig. 4b but for at 18 UT.

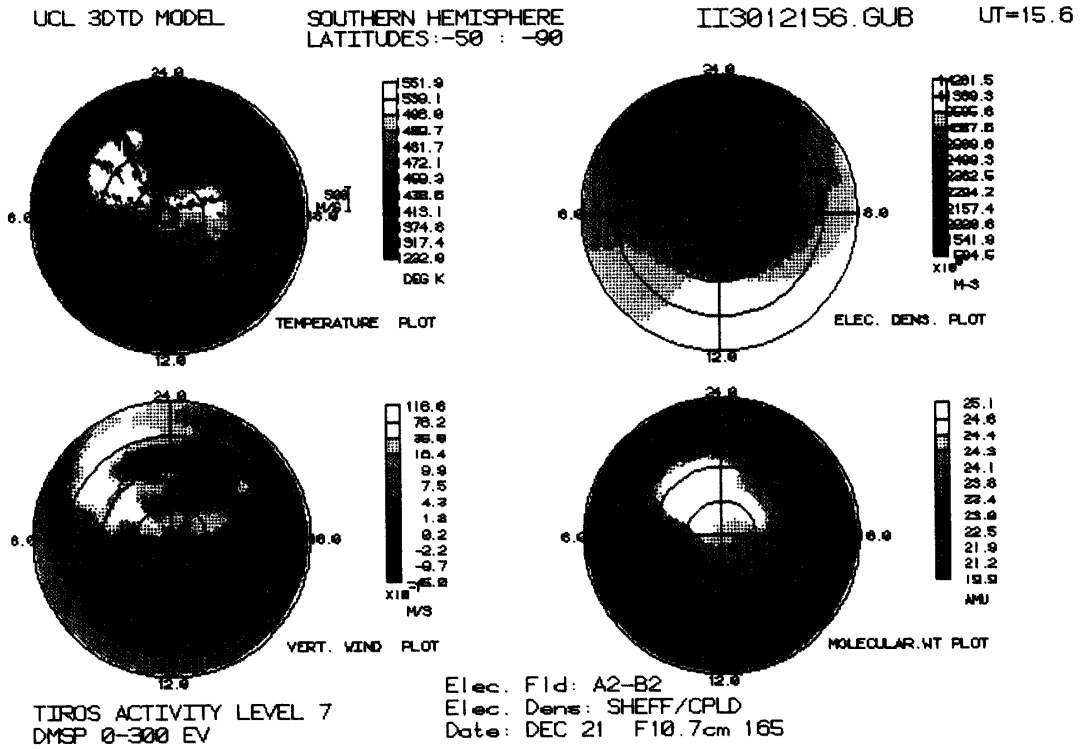

Fig. 6b. The distributions of neutral temperature, vertical wind, mean molecular mass and the ion/electron density.

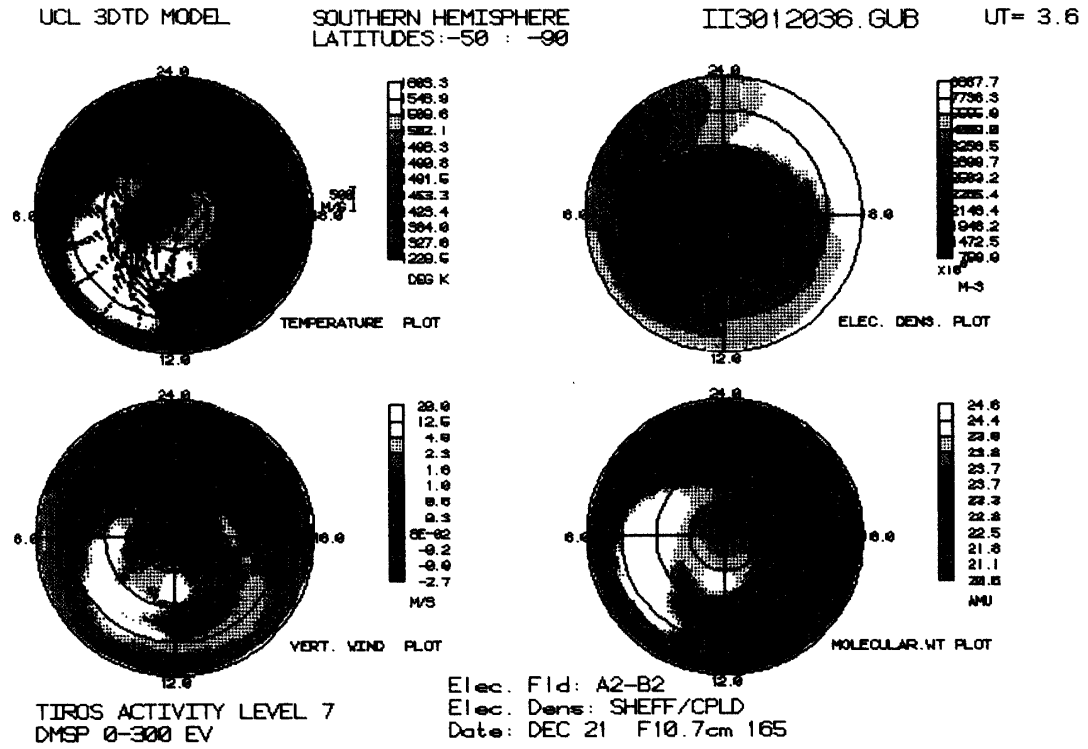

Fig. 7b. Same as Fig. 6b but for at 03.6 UT.

stagnation, a feature of the convection model they have used, which has no direct counterpart in the convection model used in this present study.

One of the effects of the UT modulation of the geomagnetic polar ionosphere, resulting from the variable solar energy and ionisation input is a surprisingly large diurnal variation in temperature within the geomagnetic polar cap. The highest temperature is in the cusp, near 18 UT, when the cusp is in sunlight, and the combination of solar and auroral ionisation causes the maximum Joule and frictional heating. Some 12 h later (06 UT), the cusp temperature has fallen by 100 K.

The seasonal dependence of ion-neutral interactions at high latitudes is illustrated in two figures showing the southern, summer, hemisphere. Figures 6 and 7 are taken from the same simulation, using the coupled ionosphere/thermosphere model for the December solstice, at 15.6 and 3.6 UT respectively. These show the region from 50° south to the geographic south pole, as viewed from above the north pole, looking downward through the earth. Using this presentation of data, it is possible to compare northern and southern polar data more easily. For example, the dawn and dusk sectors are equivalent, and the rotation of wind vectors by Coriolis acceleration appears the same, *i.e.* directed to the right. The same parameters of neutral temperature, wind and composition, and the ion density are shown for pressure level 12, close to 320 km altitude, near the *F*-region peak plasma density.

In the southern hemisphere, the geomagnetic pole is located at 16° latitude from the geographic pole at longitude 126° east. This larger offset tends to enhance the modulation of the geomagnetic input as it precesses about the geographic pole during the UT day. Generally, for the same season, larger differences in the neutral parameters would occur for these two UTs in the southern hemisphere. The present case is an exception. The difference in peak temperature between 15.6 h, a time when the geomagnetic pole is tilted away from the sun, and 3.6 h UT, a time when it is tilted towards the sun and thus receiving maximum solar heating and ionisation, is less than 50 K, contrasting with 100 K diurnal (UT) modulation for the northern winter geomagnetic pole.

This is a seasonal effect. Since most of the geomagnetic polar cap and auroral oval is in sunlight for most of the day in the southern summer hemisphere, the day/night contrast of plasma densities in the lower thermosphere is not as strong as in the winter polar region, although the absolute values are actually higher. The UT modulation of Joule heating is therefore stronger in winter (presumably also at the equinox) compared with that in summer, according to these numerical simulations. There is the apparent paradox, that the absolute Joule heating in the summer polar cap appears to be considerably greater than that in the winter polar cap, although the UT modulation is smaller.

The seasonal contrast of composition as described before is controlled by the global circulation pattern. The southern or summer polar region appears as a plateau of elevated mean molecular mass similar to that seen in the winter, both elevated as a result of the strong ion-neutral interactions (Joule and particle heating etc.). The difference between the average mean molecular mass values in the summer and winter high latitude/polar regions is large, however, around 17 amu in the winter and 23 amu in the summer.

This seasonal change in composition has a profound effect on the polar plasma densities. It has long been recognised that the seasonal mid-latitude *F*-region plasma density anomaly was casued by the seasonal change in thermospheric composition (RISHBETH and SETTY, 1961). More recently FOSTER (1984) and FARMER (1987) have shown a seasonal anomaly at high latitudes from the Chatanika and EISCAT incoherent scatter radar sites respectively. The present results indicate that this seasonal anomaly at high latitudes is reproduced by the self-consistent coupled numerical model of the thermosphere and ionosphere (FULLER-ROWELL *et al.*, 1987a, b). Comparing the polar ion density distribution at 3.6 UT in the southern hemisphere (Fig. 7), with that at 18 UT in the north (Fig. 5), times when each of the geomagnetic polar regions is respectively tilted towards the sun, illustrates that this seasonal anomaly is well reproduced.

The summer polar *F*-region ionosphere is dominated by thermospheric composition, with a very close correlation between peaks in the mean molecular mass and the troughs in ion density. This correlation even extends down to small scale features such as that at midday, 15° offset from the pole. Despite the much stronger (and continuous) solar ionising input in the summer hemisphere, the general level of polar *F*-region ion density is greater in the winter hemisphere, due to the feedback from thermospheric composition changes. Examination of Figs. 4 and 6, showing the respective UTs when both polar regions are tilted away from the sun, illustrates also that the UT modulation of the ion density exceeds the seasonal anomaly. This implies that the seasonal anomaly at high-latitudes will be strongly longitude dependent, as observed from ground-based locations, or strongly UT dependent as seen from a polar orbiting spacecraft, such as Dynamics Explorer.

One would also expect that the *F*-region seasonal anomaly would be strongly modified by the level of geomagnetic forcing. There is, as yet, no conclusive or consistent evidence of a seasonal variation in the level of auroral ionisation (EVANS, private communication, 1986). Investigation of the true seasonal anomaly therefore requires simulation of the same hemisphere at the June and December solstice, rather than comparing north and south hemispheres at one season as has been done with this initial simulation. This has added the complication of trying to untangle the effects of UT and the different offsets of the respective geomagnetic poles. These simulations will also need to be performed over a range of geomagnetic activity levels.

Finally, we note that the comparable simulations of SOJKA and SCHUNK (1985) have no such comparable composition-dominated polar depletion of plasma density. This is simply a result of their using the MSIS-83 model to define the distribution of composition. The relatively low resolution of the MSIS presentation cannot resolve the localised very large increase in mean molecular mass, and thus the compositional effect on plasma density depletion is under-estimated.

5. Longitudinal and Universal Time Asymmetries

Comparison of Figs. 4 and 5 illustrated how ion-neutral coupling at high-latitudes created the UT modulation of the wind, temperature, composition and ion density. The data are taken from the numerical simulation for the December solstice, at pres-

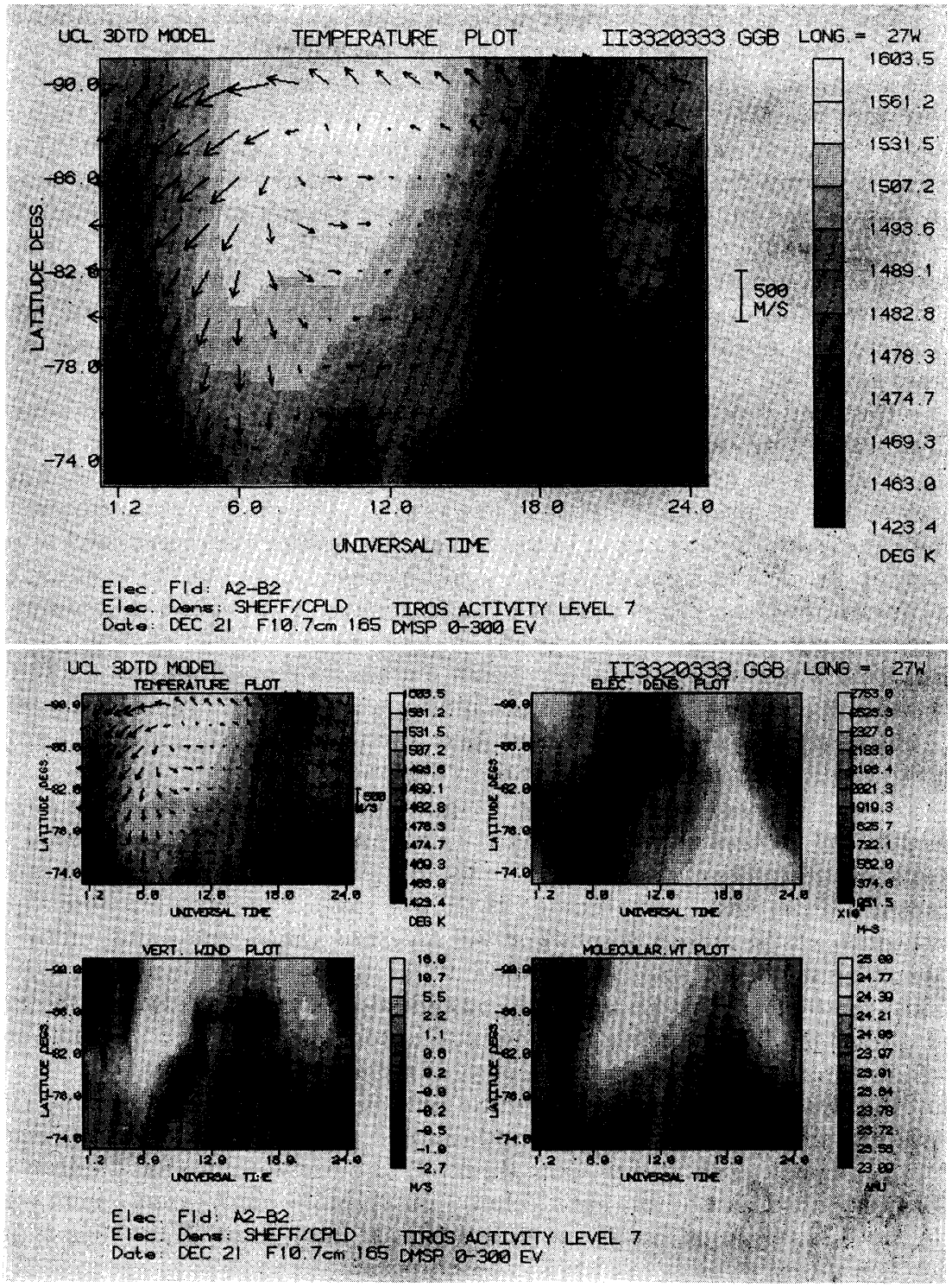

Fig. 8. The UT variation of the ionospheric and thermospheric parameters at a height of 320 km, displayed in Figs. 6 and 7, along the meridian through the Antarctic station of Halley Bay (75.5° S, 27° West Longitude). The simulation used was produced by the coupled model for the December solstice, corresponding to a geomagnetic activity level of Kp=3, and for a high level of solar activity ($F_{10.7}$ cm=185).

(a) Neutral temperature and wind distribution. (b) The distributions of neutral temperature, vertical wind, mean molecular mass and the ion/electron density.

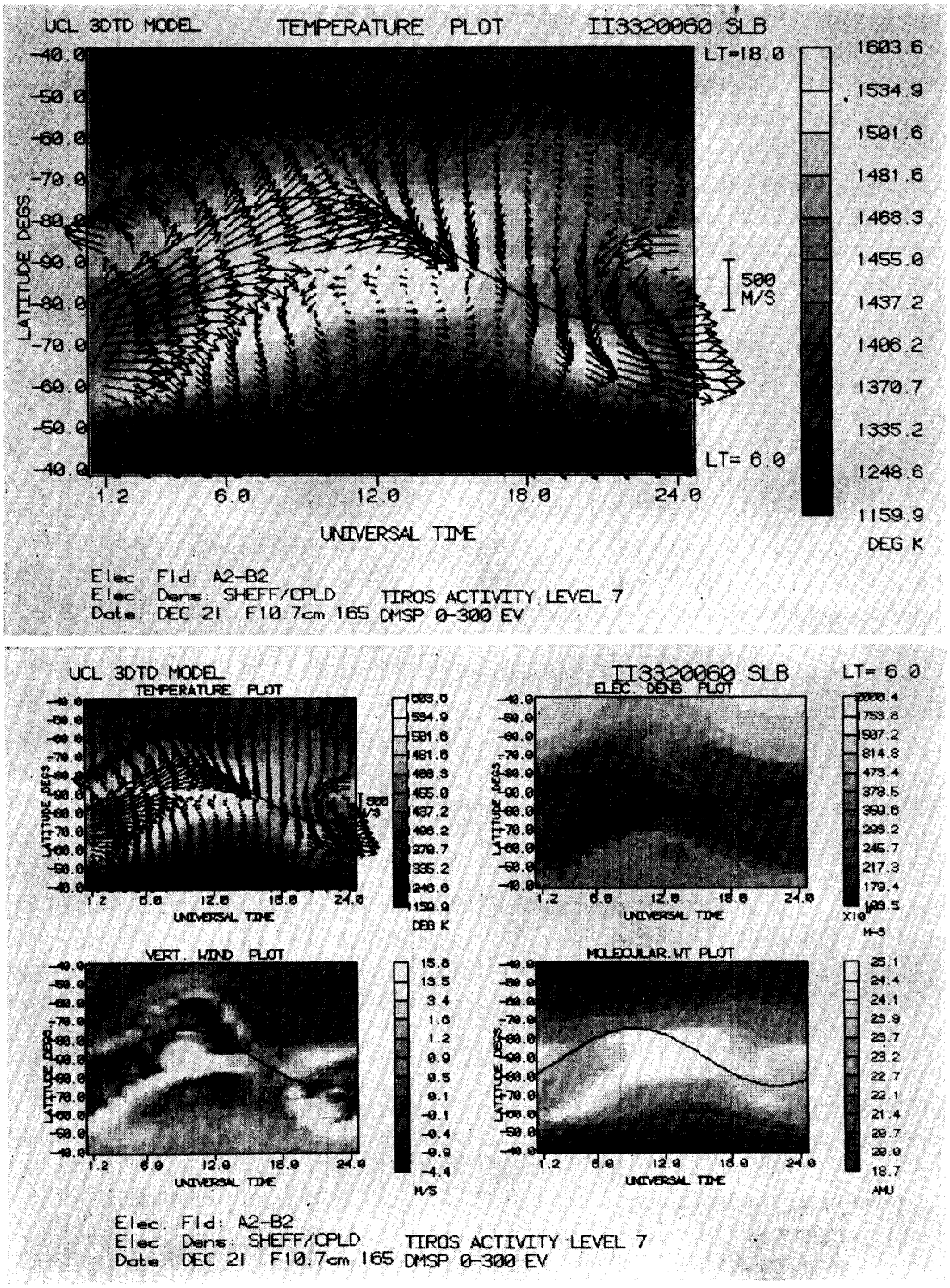

Fig. 9. The UT variation of the ionospheric and thermospheric parameters displayed in Figs. 6 and 7, as would be observed by a polar orbiting satellite, crossing the southern polar region at 320 km, with the orbit plane aligned dusk—dawn. The simulation used was produced by the coupled model for the December solstice, corresponding to a geomagnetic activity level of Kp=3, and for a high level of solar activity ($F_{10.7}$ cm=185).

(a) Neutral temperature and wind distribution. (b) The distributions of neutral temperature, vertical wind, mean molecular mass and the ion/electron density.

sure level 12, Fig. 4 corresponding to 06 UT, and Fig. 5, 12 h later, at 18 UT. At 18 UT, the geomagnetic polar cap is displaced to its maximum extent towards the dayside. Allowing for the rotation of the magnetic pole about the geographic coordinate system shown in the figures, during the 12 h period between Figs. 4 and 5, the imprints of the geomagnetic sources on the neutral temperature, vertical wind, and composition are quite similar. The peak temperature has, however, increased by 100 K at 18 UT. This is due largely to stronger solar ionisation, increasing the ion density and so increasing the Joule heating rate in the lower thermosphere. However, at the location of the temperature peak, at 65° geographic latitude on the dayside (at 18 UT), the background solar heating is also higher, compared with that at the location of the cusp at 06 UT, when it is near the geographic pole (Fig. 4).

In Fig. 8, the UT variation of the ionospheric and thermospheric parameters displayed in Figs. 6 and 7 are shown along the meridian through the Antarctic station of Halley Bay (75.5° S, 27° West Longitude). An auroral trough is observed to move rapidly equatorward, from very high southern latitudes (90° S at 22 UT), passing just equatorward of Halley in the period between 02 and 07 UT (approx.). This trough is associated with a region of elevated mean molecular mass, due to geomagnetic forcing. The trough moves rapidly poleward between 07 and 10 UT. The southern polar ionosphere in the vicinity of Halley, and poleward, is sunlit during this entire period.

The diurnal behaviour of the 'sub-auroral' trough in the summer time is quite distinct from that which occurs in the winter hemisphere, due to the different physics involved (composition changes rather than stagnation). The composition changes can be closely related to the UT times when the mean auroral oval comes closest to Halley, 21 to 06 UT, although larger-scale forcing within the entire summer polar cap region is a major factor in the depth and sharpness of the trough-like feature. We have to emphasise that this summer 'sub-auroral' trough is not a feature of plasma stagnation, but is due to molecular nitrogen enhancement caused by geomagnetic forcing. Obviously, at higher levels of geomagnetic activity, this feature will generally expand equatorward, and the structure will become more complex and time-dependent.

In Fig. 9, a view of the southern, summer, polar region is shown, as it would be viewed from a polar-orbiting satellite, such as Dynamics Explorer-2. The closest approach of the spacecraft, at each UT, to the southern geomagnetic pole is indicated by the continuous black line. The way in which the geomagnetic polar cap and auroral oval dominates the structure and dynamics of the entire polar region is extremely impressive. The correlation between the highest winds and temperatures, the highest values of mean molecular mass, the lowest plasma densities and crossings of the auroral oval/geomagnetic polar cap is dramatic. In this particular instance, the orientation of the spacecraft has been taken to be in the dusk-dawn plane (06 to 18 local solar time).

6. Major Geomagnetic Disturbances and Their Consequences

Figure 10 shows the thermospheric temperature and wind velocity distributions simulated for the June Solstice, for a major geomagnetic disturbance ($Kp=7$). In

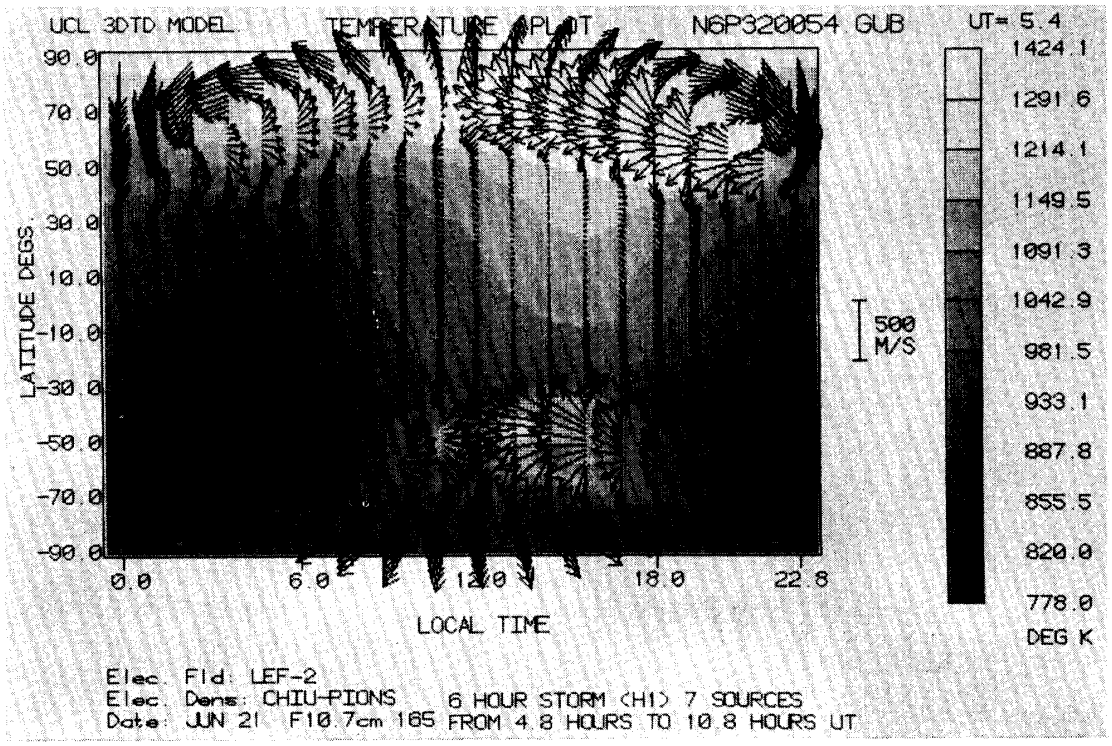

Fig. 10. The global distribution of temperature and wind at 320 km altitude 36 min after the start of a major geomagnetic disturbance. The cross-polar cap electric field is 160 kV, with an expanded auroral oval. The heating and ionising effects of energetic electron precipitation have been taken into account, although the calculations were not completed self-consistently. In addition to the major disturbances of polar winds and strong polar heating, waves can be observed to propagate rapidly toward the equator in this snap-shot.

this simulation, the geomagnetic input is time-dependent and the auroral oval diameter, cross-polar cap electric potential and auroral precipitation have all been set to be equivalent to those during an event on December 12, 1981, which was observed by DE-2 and by a ground-based interferometer in Northern Scandinavia (Rees *et al.*, 1985b). In this case, however, the simulated disturbance was started at 4.8 UT. The conditions of the June solstice were chosen, in part, as a contrast with the equivalent December simulation discussed by Rees *et al.* (1985a).

Allowing for the variation in the UT of the disturbance onset and its duration, the season and solar EUV activity, geomagnetic disturbances rarely produce larger wind magnitudes within the upper thermosphere than those depicted in this simulation. Figure 10 shows the situation some 36 min after the disturbance onset, while Figs. 11 and 12 are at intervals of 36 and 72 min (*i.e.* at 6.0 and 7.2 UT, respectively).

Progressing through these simulations, increasing temperature, density and wind enhancements are observed, primarily within the polar regions as the geomagnetic input increases. Wind systems within the auroral oval and polar cap increase greatly in magnitude, and extend equatorward as the auroral oval expands. If we discuss the northern polar region, we then consider that the southern polar region conditions are complementary. Very strong clockwise vortices are readily generated joining the dusk auroral oval and polar cap at any elevated level of geomagnetic activity.

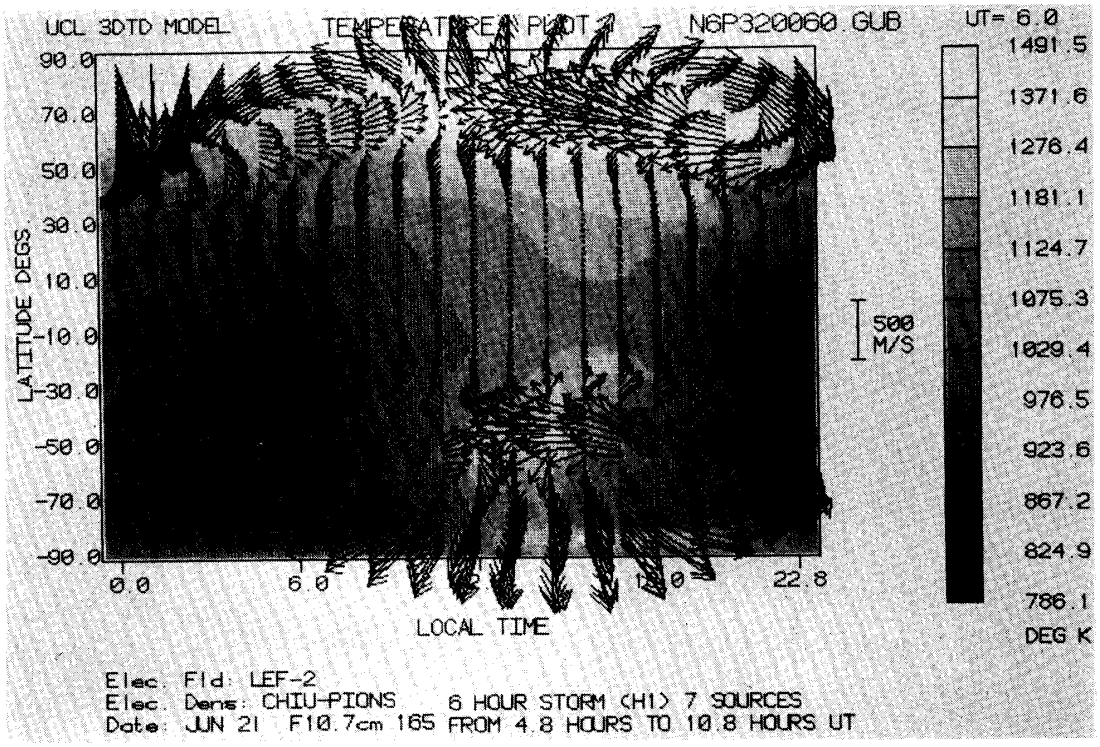

Fig. 11. As for Fig. 10, but a further 36 min into the simulated storm, the temperature wave propagating from the southern auroral oval has reached the equator. That from the northern auroral oval has reached about 20° N latitude.

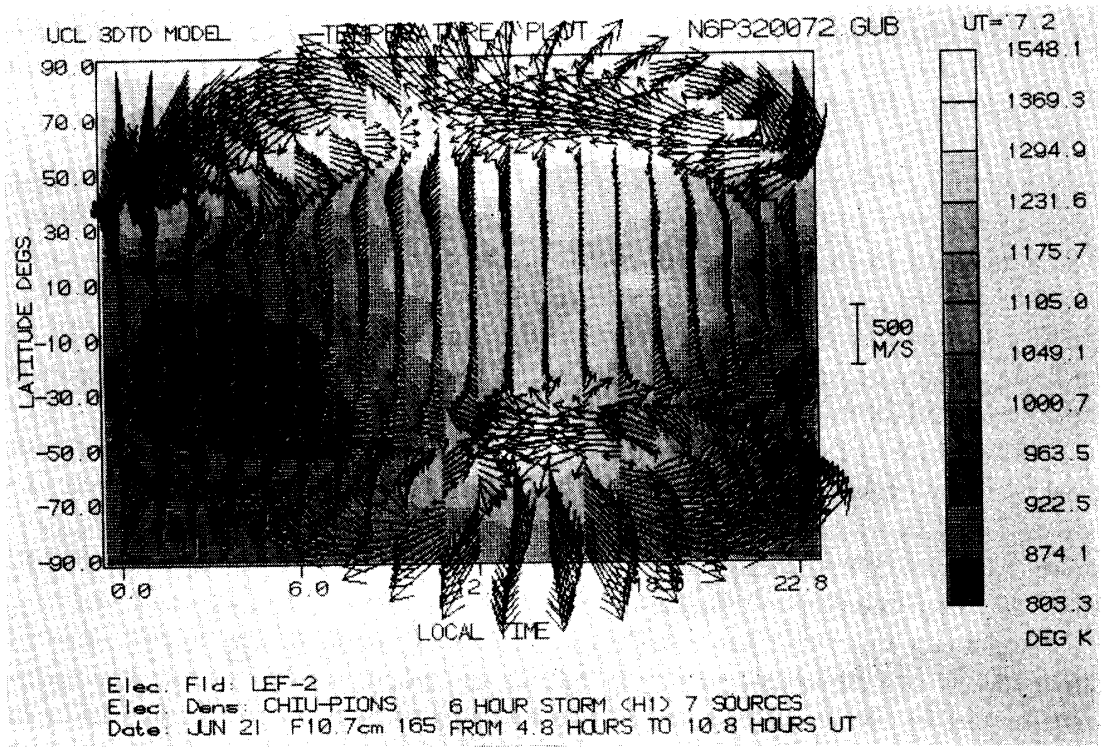

Fig. 12. As for Fig. 10, but at a time 144 min after the onset of the disturbance. The entire global thermosphere is now pervaded by waves launched from both auroral ovals (even with a rather simple time-dependence of the geomagnetic input). The primary waves launched from both auroral ovals have passed or overtaken each-other in the equatorial region.

The location of the region of strong anti-sunward flow over the polar cap depends critically on the IMF B_Y direction, as does the existence of a strong sunward wind jet within the dawn auroral oval. For IMF B_Y positive, the anti-sunward jet is on the dawn side of the polar cap, and the winds in the dawn oval are equatorward. For IMF B_Y negative, strong geomagnetic disturbances will move the anti-sunward polar cap jet to the dusk side of the polar cap, and there will be a strong sunward wind within the dawn auroral oval. Such conditions will not prevent large sunward winds occurring within the dusk auroral oval, however. While in the midnight region of the auroral oval, large equatorward winds occur at times of high activity, such winds decrease rapidly with increasing distance from the auroral oval. In general, the excitation of strong winds implies strong heating and enhancements of mean molecular mass. However, the interactions between composition changes and ionospheric chemistry are complex, and fast neutral and ion velocities also modulate the ionosphere, thus changing the nature of the forcing functions themselves.

In the time-dependent geomagnetic storm simulations, strong propagating waves are observed (Fig. 12), originating in the polar regions. In this case, the temperature waves propagating from each polar region (100 K) are large enough to be observable above background variations. Real disturbances, which have much larger spatial and temporal fluctuations than can be modelled, are likely to be significantly more effective in generating propagating wave disturbances than are the simplified simulations. Sub grid-scale structures (<200 km) and rapid time-dependent variations, which are important in real magnetospheric disturbances, have not been parameterised. The fully self-consistent model simulations produce larger mean molecular mass enhancements in the geomagnetic polar regions than the earlier non self-consistent simulation. For example, the December 21 simulation for an activity of $Kp=3$, has about the same enhancement of N_2/O ratio as the earlier storm-time simulation shown in Fig. 12.

During the initial phase of geomagnetic storms, major changes in thermospheric composition occur both at high latitudes (enhancement of molecular over atomic species) and at low latitudes (enhancement of atomic species over molecular species). The effects may be particularly pronounced in the summer hemisphere and polar region (RISHBETH *et al.*, 1985, 1987; PROLSS, 1984).

Thermospheric density responds in a complex way: There is a strong global increase in total density within the upper thermosphere in response to increases of either or both geomagnetic and solar activity. However, the detailed local response of individual species is much more complex: in general the density of the heavier and gravitationally stable species increases with both geomagnetic and solar activity. On the contrary, the densities of the lightest species (He, H), which are not completely gravitationally stable, may decrease in the upper thermosphere with increasing activity.

For very high geomagnetic disturbance levels, the auroral oval would be expanded even further equatorward than in that used for the simulation shown in Figs. 10, 11 and 12. For longer duration events, major wind disturbances tend to penetrate to greater depths within the thermosphere, as the result of viscous coupling. There is probably a significant seasonal/latitudinal asymmetry in the wind (and other) disturbances, since it appears that the summer geomagnetic polar cap is a more efficient

sink of magnetospheric energy and momentum, as ion-drag momentum transfer and Joule/frictional heating, and enhanced by higher plasma densities in the *E*-region and lower *F*-region, due to photo-ionisation in the summer geomagnetic polar regions.

Within the auroral ovals and polar caps, during very disturbed periods, at a given pressure level, the ratio of molecular nitrogen to atomic oxygen will be greatly increased. At low and equatorial geomagnetic latitudes, atomic oxygen will be enhanced over molecular nitrogen, as the result of the disturbed global circulation. Increases in the proportion of atomic oxygen, plus enhanced equatorward winds may provide a convenient answer to the middle latitude *F*-region ionospheric positive phase response to geomagnetic storms.

In the initial post-storm recovery, the dominant effects of enhanced molecular nitrogen densities within the polar regions may explain why the polar *F*-region ionosphere collapses when the additional energetic electron precipitation decays. However, as RISHBETH *et al.* (1987) have discussed, there appears to be little evidence in the theoretical global simulations to explain why the mid-latitude ionosphere should display a widely-observed post-storm negative response.

Regions of enhanced N_2 density are not carried great distances equatorward by the enhanced equatorward winds, since molecular diffusion is a very powerful restoring process once the strong geomagnetic forcing decays. One is left considering whether some quite important geomagnetic energy process are, as yet, inadequately described for their inclusion in global numerical models. Alternatively, or additionally, enhanced nitric oxide generation at high latitudes during geomagnetic storms may strongly perturb the thermal balance during the post-storm recovery of the thermosphere, by enhanced infra-red cooling. Consequent changes of wind and circulation may have quite powerful effects on thermospheric and ionospheric chemistry.

There are a number of additional complexities involved in incorporating the 'odd nitrogen' chemistry self-consistently within a theoretical three-dimensional global model. Thus it may still be some time before answers to all the outstanding questions posed by the coupled ionosphere–thermosphere system are resolved. Beyond that lies the new frontier of coupling the complex physics of the magnetosphere and of solar wind-magnetosphere interactions into the thermospheric/ionospheric models, or *vice versa*, depending on one's viewpoint and primary interests.

7. Summary

The neutral thermosphere dynamics, energy budget and composition and the ionospheric plasma density respond to a range of forcing which results in a complex observational picture, particularly within the polar regions.

In the absence of geomagnetic forcing, largely symmetric patterns would develop within the thermosphere, while the ionosphere would show significant longitudinal and interhemispheric variation due to asymmetries of the internal terrestrial magnetic field. The seasonal variations would be close to symmetric, with the northern hemisphere in June matching the southern hemisphere in December. A characteristic "summer" or "winter" response could be derived from observing either hemisphere.

The major cause of asymmetry, increasingly so at higher latitudes, is the different offset between geomagnetic and geographic poles in either hemisphere, the southern (16°) being larger than the northern (10°). Even under very quiet geomagnetic conditions, the offset geomagnetic poles cause major UT and longitudinal modulations of the polar, auroral and adjacent regions, which may appear chaotic at any time of the year. Using simulations with coupled ionospheric and thermospheric models, a number of the complexities may be unravelled.

1) A global, seasonal/latitudinal temperature gradient results from the hemispheric differences of solar UV and EUV heating of the thermosphere. The resulting pressure gradients drive a summer to winter circulation pattern, creating the latitude gradient of neutral composition. This composition structure is fundamental in explaining both mid-latitude and polar 'winter anomalies' of *F*-region ion concentration.

2) Superimposed on this global seasonal structure is a somewhat weaker (particularly for composition) diurnal variation of temperature and composition, within the mid and low-latitude regions.

3) A basic seasonal/hemispheric variation of the geomagnetic input results from the near-permanent solar illumination and ionisation of the summer polar region, and lack of such illumination of the winter pole. This enhances plasma densities in the lower altitude (*D*-region, *E*-region) ionosphere. Consequently, Joule heating in the summer polar region appears to exceed that in the winter polar region by a factor of at least 3:1.

4) The geomagnetic heat input from Joule heating and particle heating greatly modifies the global circulation, the neutral temperature and composition structure. These changes depend on geomagnetic activity, and feed back strongly into ionospheric changes, particularly those of the *F*-region.

Were the geomagnetic poles coincident with the geographic poles and the terrestrial magnetic field a pure dipole, the above effects would be highly symmetric with respect to season and latitude, and UT and longitude variations in both hemispheres would be small.

5) Even for quiet geomagnetic conditions, however, the offset poles and non-dipole terms of the terrestrial magnetic field cause major UT and longitude variations. The diurnal rotation of the earth carries the geomagnetic polar regions into locations where the solar-induced ionisation and heating is widely different. Thus, even in the absence of geomagnetic variations, polar Joule heating has a UT/hemispheric variation, as the geomagnetic polar regions are carried into and out of sunlight. The consequent UT variations of neutral temperature, dynamics, composition are quite significant, and the *F*-region ionosphere (in particular) responds not only to the changing combination of solar and geomagnetic forcing, but also to underlying changes of thermospheric composition and winds. The effects of neutral composition changes in the summer polar *F*-region are dramatic and dominant.

6) For the same season and geomagnetic activity level, the UT modulation in the southern hemisphere, thermosphere and ionosphere is always larger than in the northern hemisphere, resulting from the 16°, rather than 10°, geomagnetic polar offset.

7) The numerical simulations also indicate that the UT modulation is seasonally

and hemispherically dependent. The largest modulation would be expected at equinox, when both polar regions are carried completely into and out of sunlight each UT day.

8) At high levels of geomagnetic activity, the balance between high latitude and global (solar) energy inputs changes. The effects of geomagnetic forcing are observed to successively lower latitudes, and the effects of UT, longitudinal and hemispheric differences are exaggerated. During major storms, equivalent southern mid and low-latitude regions (geographic) may be considerably more perturbed, compared with the northern hemisphere. Depending on a ground-based or space-borne viewpoint, there will be a strong longitude or UT dependence in such disturbances.

Acknowledgements

We would like to express our thanks to S. QUEGAN, R. MOFFETT and G. BAILEY for their invaluable participation in developing the UCL/Sheffield coupled ionospheric/thermospheric model used in some of these simulations, and to J. HARMER, I. PERLA and H. HUGHES for their persistence in preparing, running and processing the many individual computer simulations. Computer time was made available by the University of London Computer Center (CRAY 1-S), and further general assistance with the project was made available by grants from the U.K. Science and Engineering Research Council.

References

AXFORD, W. I. and HINES, C. O. (1961): A unifying theory of high latitude geophysical phenomena and geomagnetic storms. Can. J. Phys., **39**, 1433–1464.

CHIU, Y. T. (1975): An improved phenomenological model of ionospheric density. J. Atmos. Terr. Phys., **37**, 1563–1570.

COLE, K. D. (1962): Joule heating of the upper atmosphere. Aust. J. Phys., **15**, 223–235.

COLE, K. D. (1971): Electrodynamic heating and movement of the thermosphere. Planet. Space Sci., **19**, 59–75.

DE LA BEAUJARDIERE, O., WICKWAR, V. B., CAUDAL, G., HOLT, J. M., CRAVEN, J. D., FRANK, L. A., BRACE, L. H., EVANS, D. S., WINNINGHAM, J. D. and HEELIS, R. A. (1985): Universal time dependence of nighttime F region densities at high latitudes. J. Geophys. Res., **90**, 4319–4332.

DICKINSON, R. E., RIDLEY, E. C. and ROBLE, R. G. (1981): A three-dimensional general circulation model of the thermosphere. J. Geophys. Res., **86**, 1499–1512.

DUNGEY, J. W. (1961): Interplanetary magnetic field and the auroral zones. Phys. Rev. Lett., **6**, 47–48.

FARMER, A. D. (1987): Extended abstract from the MIST meeting Edinburgh, April 1986. to be published in Q. J. R. Astron. Soc. London.

FOSTER, J. C. (1984): Ionospheric signatures of magnetospheric convection. J. Geophys. Res., **89**, 855–865.

FULLER-ROWELL, T. J. (1987): Numerical investigations of thermospheric/ionospheric coupling in the polar regions. to be published in Physica Scripta.

FULLER-ROWELL, T. J. and REES, D. (1980): A three-dimensional, time-dependent, global model of the thermosphere. J. Atmos. Sci., **37**, 2545–2567.

FULLER-ROWELL, T. J. and REES, D. (1983): Derivation of a conservation equation for mean molecular weight for a two constituent gas within a three-dimensional, time-dependent model of the thermosphere. Planet. Space Sci., **31**, 1209–1222.

FULLER-ROWELL, T. J., REES, D., QUEGAN, S., BAILEY, G. J. and MOFFETT, R. J. (1984): The effect of realistic conductivities on the high-latitude neutral thermospheric circulation. Planet. Space Sci., **32**, 469–480.

FULLER-ROWELL, T. J., QUEGAN, S., REES, D., MOFFETT, R. J. and BAILEY, G. J. (1987a): Interactions between neutral thermospheric composition and the polar ionosphere, using a coupled global model. to be published in J. Geophys. Res.

FULLER-ROWELL, T. J., QUEGAN, S., REES, D., MOFFETT, R. J. and BAILEY, G. (1987b): Simulations of the seasonal and universal time variations of thermosphere and ionosphere using a coupled three-dimensional global model. to be published in Pure Appl. Geophys.

HARDY, D. A., GUSSENHOVEN, M. S. and HOLEMAN, E. (1985): A statistical model of auroral electron precipitation. J. Geophys. Res., **90**, 4229–4248.

HAYS, P. B., KILLEEN, T. L., SPENCER, N. W., WHARTON, L. E., ROBLE, R. G., EMERY, B. A., FULLER-ROWELL, T. J., REES, D., FRANK, L. A. and CRAVEN, J. D. (1984): Observations of the dynamics of the polar thermosphere. J. Geophys. Res., **89**, 5597–5612.

HEPPNER, J. P. (1972): Electric field variations during substorms; OGO-6 measurements. J. Geophys. Res., **77**, 4877–4887.

HEPPNER, J. P. (1977): Empirical models of high latitude electric fields. J. Geophys. Res., **82**, 1115–1125.

HEPPNER, J. P. and MAYNARD, N. C. (1983): High-latitude electric field models. AGU Chapman Conference on Magnetospheric Currents, Irvington, Virginia, March 1983.

HINTEREGGER, H. E. (1981): Representation of solar EUV fluxes for aeronomical applications. Adv. Space Res., **1**, 39–52.

JACCHIA, L. G. (1959): Corpuscular radiation and the acceleration of artificial satellites. Nature, **183**, 1662–1663.

JACCHIA, L. G. (1961): Satellite drag during the events of November 1960. Space Res., **II**, 747–750

JACCHIA, L. G. (1977): Thermospheric temperature, density and composition; New models. Smithson. Astrophys. Obs. Spec. Rep., No. 375.

KILLEEN, T. L., HAYS, P. B., SPENCER, N. W. and WHARTON, L. E. (1982): Neutral winds in the polar thermosphere as measured from Dynamics Explorer. Geophys. Res. Lett., **9**, 977–960.

KILLEEN, T. L., HAYS, P. B., CARIGNAN, G. R., HEELIS, R. A., HANSON, W. B., SPENCER, N. W. and BRACE, L. H. (1984): Ion-neutral coupling in the high-latitude *F* region; Evaluation of ion heating terms from Dynamics Explorer 2. J. Geophys. Res., **89**, 7495–7508.

PROLSS, G. W. (1984): Local time dependence of magnetic storm effects on the atmosphere at middle latitudes. Ann. Geophys., **2**, 481–486.

QUEGAN, S., BAILEY, G. J., MOFFETT, R. J., HEELIS, R. A., FULLER-ROWELL, T. J., REES, D. and SPIRO, R. W. (1982): A theoretical study of the distribution of ionization in the high latitude ionosphere and the plasmasphere; First results on the mid-latitude trough and the light-ion trough. J. Atmos. Terr. Phys., **44**, 619–640.

REES, D. and FULLER-ROWELL, T. J. (1987a): Global thermospheric modelling. to be published in Physica Scripta.

REES, D. and FULLER-ROWELL, T. J. (1987b): Theoretical model simulations for the global thermospheric mapping study (TMS) periods. to be published in Adv. Space Res.

REES, D., FULLER-ROWELL, T. J. and SMITH, R. W. (1980): Measurements of high latitude thermospheric winds by rocket and ground-based techniques and their interpretation using a three-dimensional, time-dependent dynamical model. Planet. Space Sci., **28**, 919–932.

REES, D., ROUNCE, P. A., CHARLETON, P., FULLER-ROWELL, T. J., MCWHIRTER, I. and SMITH, K. (1982): Thermospheric winds during the energy budget campaign; Ground-based Fabry-Perot observations supported by dynamical simulations with a three-dimensional, time-dependent thermospheric model. J. Geophys., **50**, 202–211.

REES, D., FULLER-ROWELL, T. J., GORDON, R., KILLEEN, T. L., HAYS, P. B., WHARTON, L. E. and SPENCER, N. W. (1983a): A comparison of wind observations of the upper thermosphere from the Dynamic Explorer satellite with the predictions of a global time-dependent model. Planet. Space Sci., **31**, 1299–1314.

Rees, D., Charleton, P., Lloyd, N., Steen, A. and Witt, G. (1983b): Interferometric and Doppler imaging studies of the auroral thermosphere from Kiruna Geophysical Institute. Proc. VIth ESA Symposium on Rocket and Balloon Programs. ESA Publications Division, ESTEC, Noordwijk, (ESA SP-183), 53–57.

Rees, D., Lloyd, N. D., Charleton, P. J., Carlson, M., Murdin, J. and Haggstrom, I. (1984a): Comparison of plasma flow and thermospheric circulation over northern Scandinavia using Eiscat and a Fabry-Perot interferometer. J. Atmos. Terr. Phys., **46**, 545–564.

Rees, D., Smith, M. F. and Gordon, R. (1984b): The generation of vertical thermospheric winds and gravity waves at auroral latitudes—II. Theory and numerical modelling of vertical winds. Planet. Space Sci., **32**, 685–705.

Rees, D., Gordon, R., Fuller-Rowell, T. J., Smith, M. F., Carignan, G. R., Killeen, T. L., Hays, P. B. and Spencer, N. W. (1985a): The composition structure, temperature and dynamics of the upper thermosphere in the polar regions during October to December 1981. Planet. Space. Sci., **33**, 617–666.

Rees, D., Fuller-Rowell, T. J., Smith, M. F., Gordon, R., Killeen, T. L., Hays, P. B., Spencer, N. W., Wharton, L. and Maynard, N. C. (1985b): The westward thermospheric jet-stream of the evening auroral oval. Planet. Space Sci., **33**, 425–456.

Rees, D., Fuller-Rowell, T. J., Gordon, R., Smith, M. F., Maynard, N. C., Heppner, J. P., Spencer, N. W., Wharton, L., Hays, P. B. and Killeen, T. L. (1986): A theoretical and empirical study of the response of the high latitude thermosphere to the sense of the "Y" component of the interplanetary magnetic field. Planet. Space Sci., **34**, 1–40.

Rishbeth, H. and Setty, C. S. G. K. (1981): The F-layer sunrise. J. Atmos. Terr. Phys., **20**, 263–276.

Rishbeth, H., Gordon, R., Rees, D. and Fuller-Rowell, T. J. (1985): Modelling of thermospheric composition changes caused by a severe magnetic storm. Planet. Space Sci., **33**, 1283–1301.

Rishbeth, H., Fuller-Rowell, T. J. and Rodger, A. S. (1987): to be published in Physica Scripta.

Roble, R. G., Dickinson, R. E. and Ridley, E. C. (1982): The global circulation and temperature structure of the thermosphere with high latitude plasma convection. J. Geophys. Res., **87**, 1599–1614.

Roble, R. G., Dickinson, R. E., Ridley, E. C., Emery, B. A., Hays, P. B., Killeen, T. L. and Spencer, N. W. (1983): The high latitude circulation and temperature structure of the thermosphere near Solstice. Planet. Space Sci., **31**, 1479–1500.

Schunk, R. W. (1987): Interactions between the polar ionosphere and thermosphere. to be published in Physica Scripta.

Sojka, J. J. and Schunk, R. W. (1985): A theoretical study of the global F region for June solstice, solar maximum, and low magnetic activity. J. Geophys. Res., **90**, 5285–5298.

Sojka, J. J., Raitt, W. J. and Schunk, R. W. (1979): Effect of displaced geographic and geomagnetic poles on high-latitude plasma convection and ionospheric depletions. J. Geophys. Res., **84**, 5943–5951.

Sojka, J. J., Raitt, W. J. and Schunk, R. W. (1981): A theoretical study of the high-latitude winter F region at solar minimum for low geomagnetic activity. J. Geophys. Res., **86**, 609–622.

Spiro, R. W., Reiff, P. F. and Maher, L. J. (1982): Precipitating electron energy flux and auroral zone conductances—an empirical model. J. Geophys. Res., **87**, 8215–8227.

Stewart, R. D., Smith, R. W., Rees, D., Dudeney, J. R. and Rodger, A. S. (1985): First measurements of thermospheric winds in Antarctica by an optical ground-based method. Nature, **317**, 45–47.

Torr, M. R., Torr, D. G. and Hinteregger, H. E. (1980): Solar flux variability in the Schumann-Runge continuum as a function of solar cycle 21. J. Geophys. Res., **85**, 6063–6068.

(Received October 13, 1986; Revised manuscript received March 3, 1987)